Fuel 422 (2026) 139080

Contents lists available at ScienceDirect

Fuel

journal homepage: www.elsevier.com/locate/jfue

Full length article

Computational study of the formation, migration, and decomposition of epoxy groups during the combustion of char

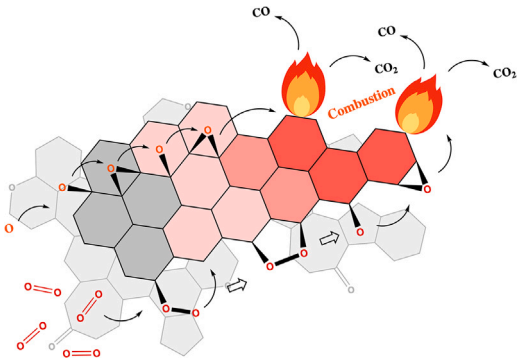
Bastian Schnieder[a,*], Babak Farhadi Jahromi[b], Rochus Schmid[b], Christof Hättig[a]

[a] Ruhr-Universität Bochum, Lehrstuhl für Theoretische Chemie, 44780 Bochum, Germany
[b] Ruhr-Universität Bochum, Lehrstuhl Anorganische Chemie 2, Computational Materials Chemistry Group, 44780 Bochum, Germany

HIGHLIGHTS

- Two primary pathways for epoxide formation on char surfaces are revealed: via peroxo-bridge intermediates and direct atomic oxygen addition.
- Density functional theory calculations show low energy barriers for epoxide migration, indicating significant surface mobility during char oxidation.
- Structural defects on the char surface promote the transformation of epoxides into more stable oxygenated species like ethers and lactones, supporting experimental XPS findings.

GRAPHICAL ABSTRACT



ARTICLE INFO

Keywords:
Char
Combustion
Epoxides
Mechanism
GFN2-xTB
DFT
XPS

ABSTRACT

Char is considered as one of the most promising base-load fuels for sustainable heat and power generation. Recent XPS studies have identified epoxides as some of the most abundant oxygen functional groups during the initial oxidation stage of raw char. These surface oxides are highly reactive and have been reported to migrate across the surface, converting into ethers, lactones, and other oxygenated species at temperatures above 500 °C.

The present study investigates the formation, surface mobility, and subsequent transformation of epoxides in char by means of molecular dynamics simulations that are applied to several molecular models, employing the GFN2-xTB method for the potential energy surface. To determine activation and reaction energies of the key reaction pathways we employ density functional theory with the TPSSh functional and the def-TZVP basis set.

We identify two primary epoxide formation pathways: (i) the addition of molecular oxygen to edge radical sites, forming peroxo-bridges that subsequently cleave into alkoxy radicals and epoxides, and (ii) the direct addition of atomic oxygen to the char surface. We find low energy barriers for surface migration, indicating high mobility of epoxides. Additionally, in agreement with experimental observations, we find that structural defects can drive the conversion of epoxides into ethers and lactones.

Our results highlight the role of epoxy groups as surface oxides in the heterogeneous combustion of raw char.

* Corresponding author.
Email address: bastian.schnieder@ruhr-uni-bochum.de (B. Schnieder).

https://doi.org/10.1016/j.fuel.2026.139080
Received 30 September 2025; Received in revised form 13 February 2026; Accepted 6 March 2026
Available online 18 March 2026
0016-2361/© 2026 The Authors. Published by Elsevier Ltd. This is an open access article under the CC BY license (http://creativecommons.org/licenses/by/4.0/).

1. Introduction

The global shift toward sustainable heat and power generation has highlighted biochar as a promising alternative to fossil fuels [1–3]. Pyrolytic conversion processes produce in addition to syngas and bio-oil, carbon-rich char (charcoal) as a suitable base-load fuel for electricity and heat generation [3,4]. Many combustion studies have aimed to uncover the chemical nature of various heteroatomic functional groups [5,6], with oxygen being the most abundant heteroatom in the carbon structure of biomass-derived fuels [7]. During combustion in oxygen-containing atmospheres, char is converted into carbon dioxide (CO_2) and carbon monoxide (CO) [8,9]. Molecular oxygen (O_2) or oxygen-containing radicals such as hydroxyl radicals (HO•) react at the edge of the carbon structure, forming highly reactive oxo-carbon intermediates [10,11]. Among these reactive intermediates, epoxides are reported to form particularly below 500 °C [5].

Cerciello et al. [12] investigated experimentally the evolution of oxygen functional groups in raw char samples at different temperatures using X-ray photoelectron spectroscopy (XPS). They put forward the hypothesis that epoxides are one of the most abundant oxygen-containing groups formed during the initial oxidation stage [12] and transform at higher temperatures into other oxygen functional groups such as pyrans and lactones. Although it is experimentally proven that epoxides form or temporarily exist in the carbon framework of chars during combustion, the molecular mechanisms leading to the formation of these surface epoxides remain poorly understood.

An early contribution to the mechanistic insights was made by Incze et al. [13] using periodic density functional theory (DFT) calculations on graphite, which was populated with different amounts of atomic oxygen. By considering various sites for the population, it was found that direct placement on top of C–C bonds, leading to epoxy groups, is thermodynamically favored [13]. Furthermore, the intercalation of atomic oxygen into graphite was found to lead to more stable configurations than addition to the surface [13]. Later, Sánchez et al. [14] proposed reaction pathways that include epoxide formation reactions in a computational study that aimed at the mechanistic understanding of CO_2 evolution during char oxidation. They employed DFT calculations on a hydrogen-terminated graphene fragment with an unsaturated edge, used as a model for char. They observed that after consecutive addition of molecular oxygen to carbon atoms at the unsaturated edges, an epoxy group is formed on the basal plane of the graphene model. They proposed a reaction pathway with reasonable activation barriers that leads to the transformation of the epoxy group into a cyclic ether at the oxidized edge of the model system under CO_2 elimination. Orrego et al. later published a follow-up study that focused on the naphthoxy radical [15]. This study showed that the addition of atomic oxygen ($O(^3P)$) at the edge of the aromatic ring system can also initiate reaction pathways that lead to CO_2 elimination. The formation of epoxides on the basal plane was identified as a key intermediate step in this process. Following this, Radovic et al. conducted a DFT-based study on a number of finite model systems and (periodic) graphene. They also observed surface epoxide formation via addition of oxygen species at reactive edge sites, such as carbenes, followed by spillover to the basal plane [16,17].

The aforementioned studies, which relied on human-guessed reaction mechanisms, have contributed significantly to the mechanistic understanding of epoxide formation and migration on graphenic surfaces. In the present work, we elaborate on this matter by taking a more systematic approach toward the identification of relevant reaction mechanisms. We employ reactive molecular dynamics (MD) simulations for reaction discovery, followed by a refinement of the discovered reactive species and pathways with accurate DFT calculations using the automated workflow developed by Schmitz et al. [18]. In the refinement, we employ state-of-the-art exchange-correlation functionals and adequately sized basis sets to guarantee high quality thermodynamic and kinetic results. We study three model systems, depicted in Fig. 1 and discussed further in Section 2.1, that display some of the geometric and compositional aberrations, that distinguish char from graphite [19].

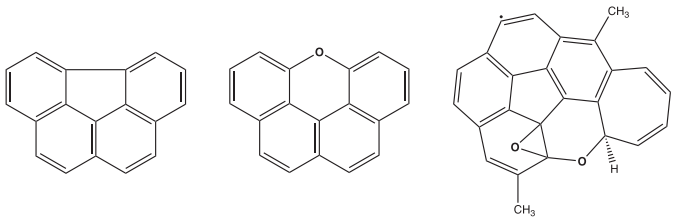


Fig. 1. Lewis structures of the constructed char molecules. System **A**: benzo[*ghi*]fluoranthene, **B**: naphtho[2,1,8,7-*klmn*]xanthene, **C**: 1,7-dimethyl-11a*H*-12a,12a^1-epoxybenzo[4,5]fluoreno[1,9,8-*cdef*]cyclohepta[*ij*]isochromen-5-yl radical.

For the present study, we modified the original reaction discovery workflow by changing the employed energy model for the MD simulations from the reactive force field model ReaxFF [20] to the extended tight binding method GFN2-xTB [21]. Although widely applied in computational investigations of combustion and pyrolysis processes [22–24], ReaxFF was found in preliminary test calculations—summarized in the supplementary material to the present study [25]—to be incapable of describing the formation of surface epoxides. Specifically, ReaxFF overestimates the barriers for epoxide formation via O_2 addition by up to 120 kJ/mol compared to DFT reference values. In contrast, GFN2-xTB reproduces these barriers much more accurately. The validity of the GFN2-xTB method for high temperature conversion of aromatic hydrocarbons was recently demonstrated in the context of soot formation by Cong et al. [26]. To the best of our knowledge, this represents a novel approach in combustion studies and enables the exploration of reaction pathways that are unavailable in ReaxFF MD simulations.

We report the formation and decomposition mechanisms of epoxide groups, as well as thermodynamic data on their stability and reactivity. Furthermore, we provide results for shifts in the binding energies of the oxygen 1*s* core orbitals in ethers and epoxides that can be compared with experimental data from XPS spectroscopy which is widely used to identify oxygen surface groups in coal, char, or carbon-based residues. In the context of oxygen functional groups, XPS shifts allow one to distinguish between carbonyls, carboxylic acids, or epoxy groups [27,28]. The core-level shifts reported in this work can be used as a computational reference for experimentally measured XPS spectra of char and related materials.

2. Methods

2.1. Char molecule construction

The model systems shown in Fig. 1 were derived from larger char models constructed using our previously developed methodology for generating realistic char models, as described by Angenent et al. [29,30]. The model systems **B** and **C** contain oxygen functionalities, whereas **A** represents pure polyaromatic hydrocarbon regions. System **C** includes pre-existing radical sites to promote early addition events in the simulations. This is motivated by literature reports which suggest that hydrocarbon combustion is typically initiated by hydrogen abstraction reactions that lead to the formation of intermediate edge radicals [31,32]. Furthermore, system **C** contains a surface-bound epoxide, which enables the study of possible migration reactions along the surface, removing the dependence on dynamic epoxide formation. This system is specifically chosen to investigate epoxide migration on char-like surfaces that feature multiple aromatic deficiencies and aliphatic (–CH_3) side chains.

2.2. Molecular dynamics simulations

All MD simulations were performed with the Large-scale Atomic/Molecular Massively Parallel Simulator (LAMMPS) program package [33] through the pylmps interface [34], which is interfaced to the xtb program package [35] and provides the GFN2-xTB [21] energies and forces. We considered several simulation environments for the char flakes. For systems **A** and **B**, we investigated their reaction dynamics in the presence of a single $O(^3P)$ radical, which was placed in the vicinity of the flake during setup. Respectively, ten independent MD simulations of this type were performed, all at 1500 K and without explicit boundary conditions or any additional spatial constraints. For system **C**, two different simulation environments were considered. Firstly, the bare flake was simulated in vacuum, i.e., without boundary conditions and without including other reactants, once at 1500 K and once at 2000 K. Secondly, a simulation of **C** in an O_2 atmosphere was performed at 1500 K. The latter was set up by placing the char model **C** in the center of a cubic box with a side length of 25 Å and populating the vacant space in the box with 12 O_2 molecules at random positions using the PACKMOL software package [36]. To retain the O_2 atmosphere in the MD simulation, we employed the spherical nanoreactor approach described by Grimme [37]. In this method, the simulated system is confined by a spherical potential, as illustrated in Fig. 2, which increases the number of intermolecular collisions and thereby the frequency of reaction events. The enhanced reactivity partially compensates for the higher computational cost of GFN2-xTB compared to ReaxFF. The nanoreactor potential was constructed by defining a sphere with a radius of 23 Å, placed with its center at the origin of the simulation cell, and adding a penalty to the systems potential energy for every atom that leaves the sphere. The penalty potential was set to zero within the sphere and defined as a quadratic function of the distance of the respective atom from the surface outside the sphere, ensuring continuity of both the potential energy and the forces. A harmonic force constant of 10 kcal $mol^{-1}Å^{-2}$ was used for the penalty potential. Beyond the nanoreactor potential, no explicit boundary conditions were employed.

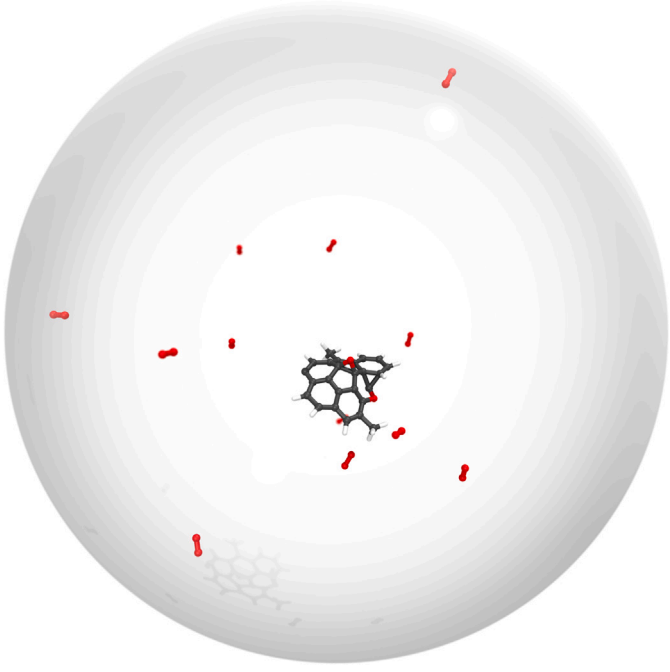


Fig. 2. Illustration of the nanoreactor setup in an MD simulation of **C** in an O_2 atmosphere. The nanoreactor region is indicated by a transparent sphere with a radius of 25 Å.

All simulations were carried out with an integration time step of 0.1 fs and with an electronic spin equal to the sum of the number of present oxygen atoms and aryl radicals. The electronic temperature was always set to the respective target temperature of the system. Each simulation run consisted of a heating stage followed by a production stage. In the heating stage, the atomic velocities were initialized randomly from a Gaussian distribution to yield an initial temperature of 300 K. A Berendsen thermostat [38] was then applied to heat the system to the target temperature over 4 ps with a linear ramp during the first 2 ps and a constant target temperature during the second 2 ps. In the nanoreactor simulations, this stage served the additional purpose of dynamically restraining the O_2 molecules within the nanoreactor sphere. In the production stage, the heated system was propagated for 1 ns at constant temperature using chained Nosé-Hoover thermostats [39–42] with a chain length of 5.

All MD trajectories were analyzed using our in-house workflow program described in Ref. [18]. For this study, the findR code was extended to compute bond orders based on a suggestion by Grimme et al. [43]. The program findR identifies reaction events in a trajectory and automatically refines them at the DFT level. The identification of reaction events is based on a graph-theoretical analysis that screens the trajectory stepwise for changes in the (undirected) molecular graph of the char model. Detected reaction events are stored in a database and initially optimized at the DFT/TPSS-D3/def-SVP level. If the molecular graph remains consistent after this optimization, the corresponding reactants, products, and transition states are further optimized at the higher DFT/TPSSh-D3/def-TZVP level.

2.3. Electronic structure calculations

All electronic structure calculations were performed using the TURBOMOLE program package (version 7.6) [44]. The reactions tracked in the MD trajectories were refined with density functional theory (DFT) as a commonly used method to calculate reaction energies and barriers [45]. For the DFT calculations the resolution-of-the-identity (RI-J) approximation [46] was used with optimized auxiliary basis sets [47] for the Coulomb matrix, and Grimme's D3 dispersion correction [48] was included. In the first step, the structures from the high-temperature MD trajectory were optimized with the TPSS meta-GGA functional [49] and the def-SVP [50] basis set. To obtain more accurate geometries and electronic energies, a second refinement was performed using the meta-hybrid TPSSh functional [51] and the def-TZVP [52] basis set. The electronic reaction and activation energies (barriers) were calculated with Eqs. (1) and (2), respectively. The subscript TS denotes the transition state for a given reaction and the index i is used for equilibrium geometries.

$$E_{\mathrm{rxn}} = \sum_{i}^{\mathrm{products}} (E_{\mathrm{el},i} + E_{\mathrm{ZPV},i}) - \sum_{i}^{\mathrm{reactants}} (E_{\mathrm{el},i} + E_{\mathrm{ZPV},i}) \tag{1}$$

$$E_{\mathrm{act}} = E_{\mathrm{el,TS}} + E_{\mathrm{ZPV,TS}} - \sum_{i}^{\mathrm{reactants}} (E_{\mathrm{el},i} + E_{\mathrm{ZPV},i}) \tag{2}$$

Zero-point vibrational energies E_{ZPV} were scaled by the factor of 0.9874 for a TPSSh functional reported in Ref. [53], and added to the electronic energies E_{el}. Reaction pathways were generated and optimized using the chain-of-states method implemented in the woelfling module [54] of TURBOMOLE. The final transition-state structures were further optimized with the trust-region image minimization algorithm [55] (statpt module) and validated by intrinsic reaction coordinate calculations (DRC module [56]).

To compute the core-level shifts of the oxygen 1s orbitals, molecular orbital eigenvalues were used to estimate the binding energies according to Koopmans' theorem. This approximation allows only for a qualitative estimate of the binding energy, as it neglects contributions from orbital relaxation [57,58]. For open-shell systems, the eigenvalues of the α-spin MOs were used. The XPS shifts were computed at the DFT TPSSh-D3

level using the def-TZVP [52], and cc-pV5Z [59] basis sets for molecular geometries optimized at the same respective level of theory. All shifts are reported relative to the $1s$ binding energy of the epoxide oxygen in the reference systems used also in Ref. [5], to ensure consistent comparison with the results from the latter work.

2.4. Visualization

The rendering of MD structures was realized using the Visual Molecular Dynamics (`VMD`) program package [60] in combination with the ray tracing library Tachyon [61]. All Lewis structures were visualized using the `ChemDraw` [62] software tool, and the corresponding energy diagrams were generated using the `mechaSVG` [63] program package.

3. Results and discussion

The trajectories of the GFN2-xTB MD simulations revealed two possible formation pathways for epoxide groups, starting with the addition of either $O(^3P)$ or O_2 to the char model. Furthermore, we observed that epoxides tend to decompose into ethers or lactones at the edge of the char model. The underlying mechanisms will be discussed in the following.

3.1. Epoxide formation and migration

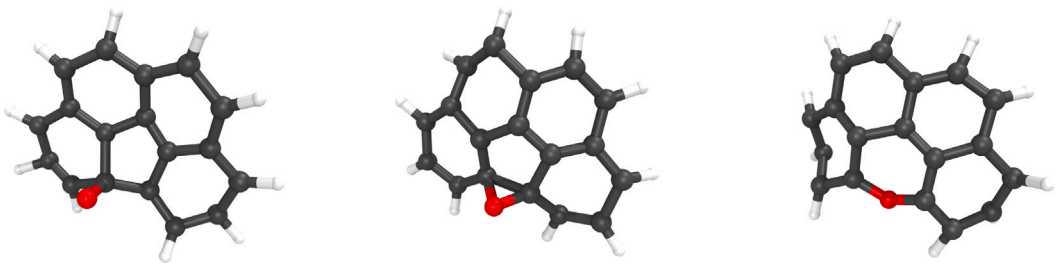
Char is a non-homogeneous, graphene-like residue characterized by various geometric distortions and defects in the aromatic ring systems [19,64]. To capture these effects, we used model system **A**, which contains a ring deficiency defect and a sufficiently large π-system to allow both epoxide formation at different sites and subsequent epoxide migration. MD simulations with GFN2-xTB were performed for system **A** in the presence of a single $O(^3P)$ atom at 1500 K to study epoxide formation and migration. We assume the presence of reactive radical species, such as molecular oxygen (O_2) and atomic oxygen, in the combustion atmosphere. In addition to O_2, atomic oxygen plays a crucial role in combustion chemistry [65], and simulations show that it readily forms addition products with the char system. In the first reaction step, $O(^3P)$ attaches to the surface of system **A**, forming alkoxy radicals (**A2**, **A6**, and **A8**). In subsequent steps, the oxygen atom migrates to vicinal carbon atoms and reacts to form epoxy functional groups (**A3**, **A5**, **A7**, and **A9**). An exemplary MD trajectory in which this mechanism was observed is shown in Fig. 3, where the intermediate species and the simulation time at which they were formed are displayed.

The epoxide migrates on the surface of **A** throuh sequences of C-O bond dissociation, leading to alkoxy intermediates, followed by formation of a new C-O bond with a neighboring C atom. The MD simulations further revealed that the epoxy oxygen atom can insert into a carbon ring through the dissociation of the epoxy C–C bond, resulting in intermediate ether structures (**A4**, **A10**, and **A11**). Examples for the reaction steps involved in these two types of events — migration and ring insertion — are shown in Fig. 4.

A schematic overview of all discovered epoxide formation and migration pathways is depicted in Fig. 5. The corresponding refined reaction energies and activation barriers, relative to the reactants (**A1** + $O(^3P)$), are presented in Fig. 6. These results reveal that the addition of $O(^3P)$ to the surface of **A** is a barrierless process, with reaction energies ranging from −47.8 to −76.8 kJ/mol, depending on the reaction site. All epoxide formation reactions are exothermic relative to the initial reactants. The elementary reaction steps with the highest barriers are the formations of ether bridges that yield seven-membered rings. For example, the conversion of **A5** to **A4** requires an activation energy of 93 kJ/mol and leads to a structure that is 33 kJ/mol higher in energy than the initial reactants (Fig. 6). In contrast, the insertion of the O atom into a five-membered carbon ring to form a pyran group is highly exothermic, releasing −247 kJ/mol. This suggests that the epoxides tend to migrate toward geometric defects—such as five-membered rings—and convert to ether (C–O–C) bridges.

The relaxation of the pyran **A10** to its singlet state yields system **B**. Similar to system **A**, nanoreactor simulations with **B** exposed to an $O(^3P)$ atom were performed and analyzed. In these simulations, $O(^3P)$ was observed to add to various sites on **B**, followed by frequent migration events of the resulting epoxy groups on the surface. The discovered reaction pathways initiated by the addition of $O(^3P)$ to **B** are shown in Fig. 7, and the corresponding refined energy profile is presented in Fig. 8. As previously observed for **A**, all oxygen addition reactions are barrierless. Thermodynamically, the most favorable pathway is the direct addition leading to species **B11**, releasing an energy of –97.6 kJ/mol relative to the reactants. Additionally, species **B7** is a thermodynamically favorable intermediate, with an energy of –96.0 kJ/mol compared to the reactants. Species **B7** was further investigated manually to explore the formation of a corresponding lactone functional group, yielding species **B8**. All reaction events depicted in Fig. 7 exhibit low energy barriers and are, with the exception of the conversion of **B4** to **B9**, exothermic. These low barriers support the hypothesis of Levi et al. [5] that epoxy groups exhibit high surface mobility especially at elevated temperatures in the early stages of combustion processes. The energy profiles (Figs. 6 and Fig. 8) further indicate that in the presence of pyran rings epoxides can also convert to lactones. For system **B**, this is an exothermic reaction releasing −52.2 kJ/mol. We note, that no minimum on the DFT TPSSh-D3/def-TZVP energy surface was found for the species **B6**, which was observed in the MD trajectory.

The direct chemisorption of O_2 has been reported to lead to surface oxides, where oxygen atoms are covalently bonded to the char surface itself [12,66,67]. The reaction of carbon with O_2 typically begins with its addition to the carbon backbone, preferably at edges and defect sites



(a) 1.25 ps: Oxygen addition. (b) 1.35 ps: Epoxide formation. (c) 1.42 ps: Ether formation.

Fig. 3. An exemplary epoxide formation mechanism for model system **A**, initiated by the addition of $O(^3P)$. Found in a GFN2-xTB MD trajectory for 1500 K with a nanoreactor setup.

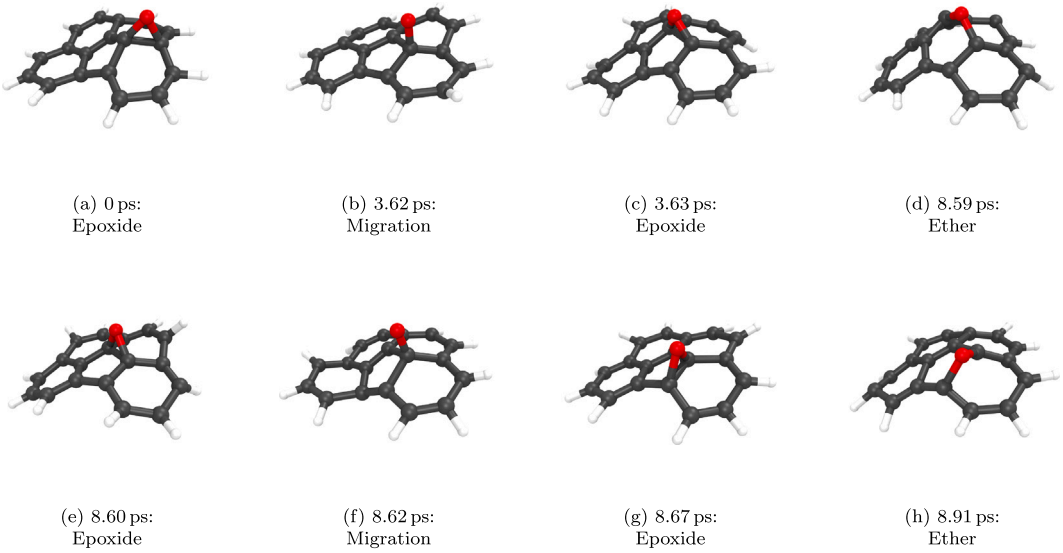


Fig. 4. An exemplary epoxide migration mechanism in **A** after addition of O(^{3}P) and subsequent epoxide formation, discovered in a GFN2-xTB simulation conducted at 1500 K in a nanoreactor setup.

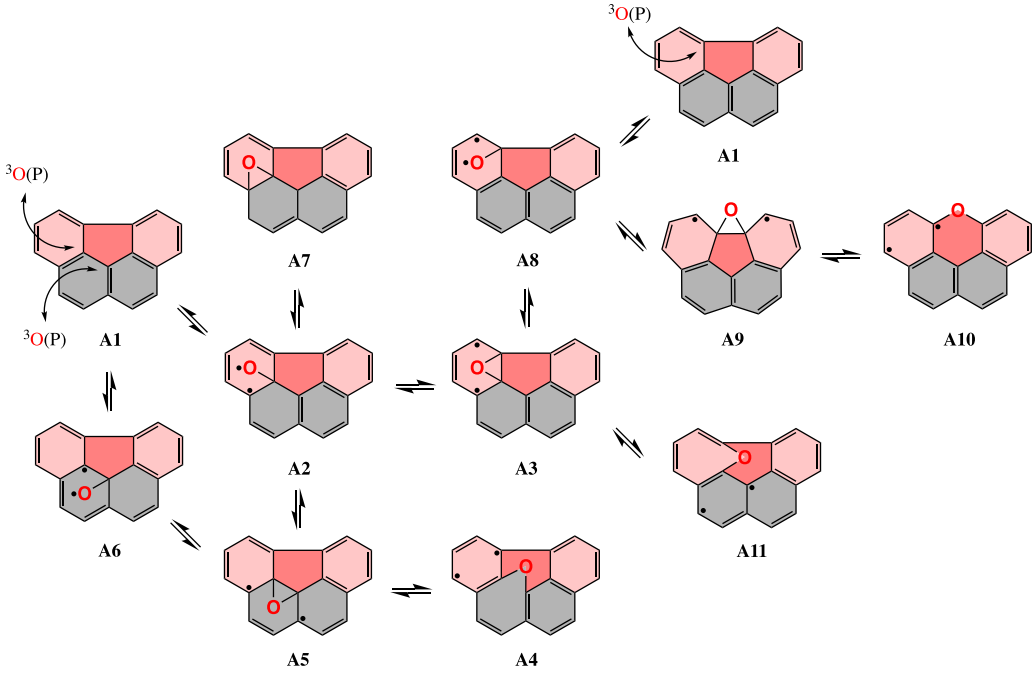


Fig. 5. Epoxide formation and migration reactions resulting from the addition of atomic oxygen onto benzo[ghi]fluoranthene, as observed in GFN2-xTB nanoreactor simulations at 1500 K. The two unpaired electrons ($M_S = 3$) are delocalized within the π-system. For clarity and compactness, the structures are depicted in one of their mesomeric resonance forms.

such as carbon-centered radicals [68,69]. In the nanoreactor simulations of system **C**, containing such a radical site, in O_2 atmosphere, the addition of O_2 to the radical site was indeed observed, as seen in the MD snapshot shown in Fig. 9(a). The addition of O_2 to an aryl radical site leads to a peroxo radical which subsequently reacts first with a neighboring carbon atom to form a five-membered ring (Fig. 9(b)) before the O–O bond breaks and an alkoxy radical forming an epoxide group (Fig. 9(c)). The existence of edge peroxyl groups has been reported for aliphatic chains (alkanes) during autoxidation events. In the present work, we observed only the addition of peroxyl groups to neighboring rings, rather than hydrogen atom abstraction as observed in previous combustion studies [11,69]. While we cannot rule out the occurrence of hydrogen abstraction reactions, we did not further pursue these paths as the focus of this study is the formation and mobility of epoxy groups.

The refined energy profile for this epoxide formation pathway is shown in Fig. 10. The formation of the epoxide group from the arylperoxo radical is a two-step mechanism where the first step, the formation of the peroxo bridge (**C2** with a barrier of 110.3 kJ/mol is the time-determining step. The subsequent rearrangement to an aryloxo radical and an expoxide has a small barrier of 20.0 kJ/mol and releases −152.6 kJ/mol.

To confirm that this epoxide formation pathway is not an artifact of the complex chemical and electronic structure of the model system **C**, we investigated it also for a less complex system (**D**), shown in Fig. 11. The

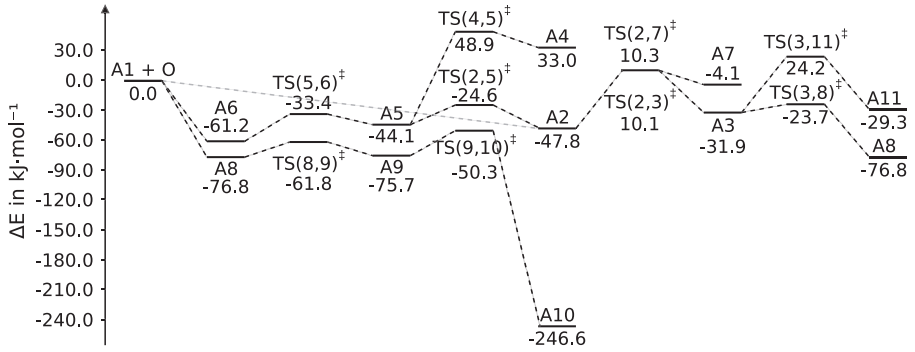


Fig. 6. Reaction profile of system **A** with O(^{3}P) (Fig. 5). Reaction energies and barriers (TS) are given relative to the reactants at DFT/TPSSh-D3/def-TZVP level in kJ/mol. The light gray lines mark the direct addition of atomic oxygen at different sites.

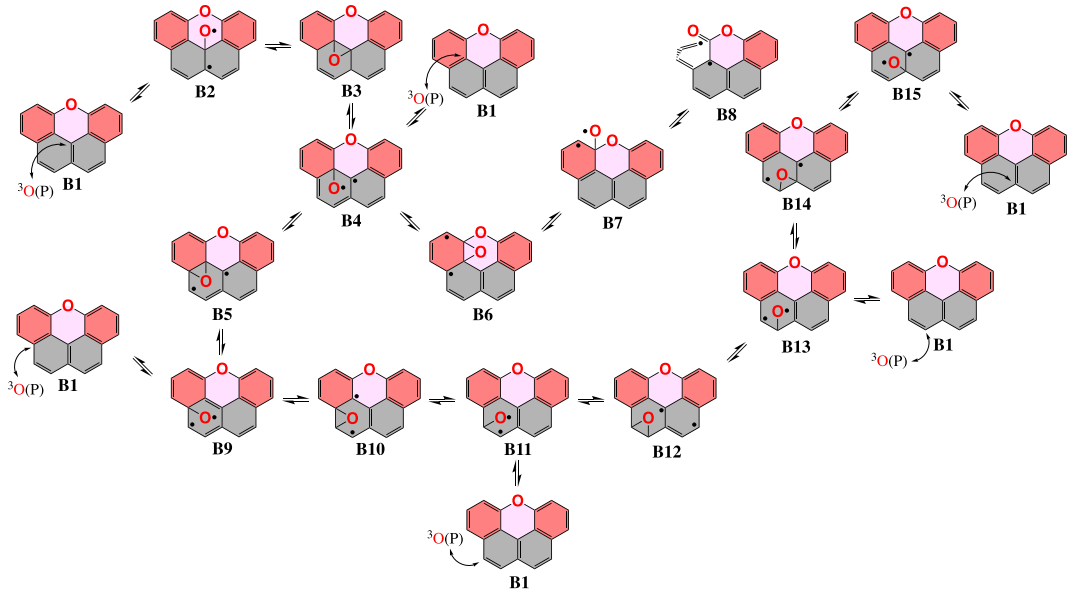


Fig. 7. Epoxide formation and migration reactions initiated by the addition of O(^{3}P) to **B**, as observed in GFN2-xTB nanoreactor simulation at 1500 K. The two unpaired electrons ($M_S = 3$) are delocalized within the π-system. For clarity and compactness, the structures are depicted in one of their mesomeric resonance forms.

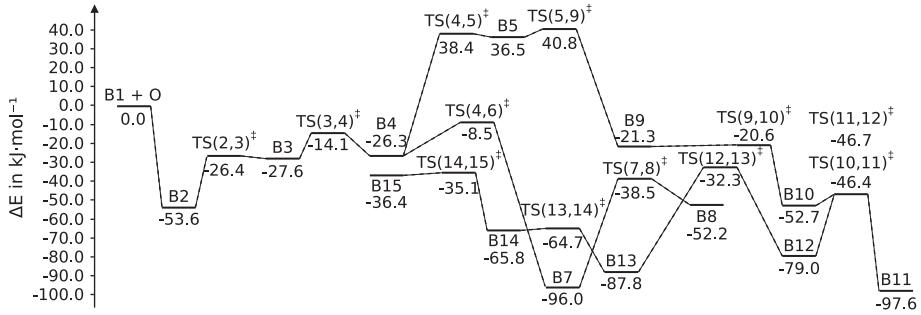
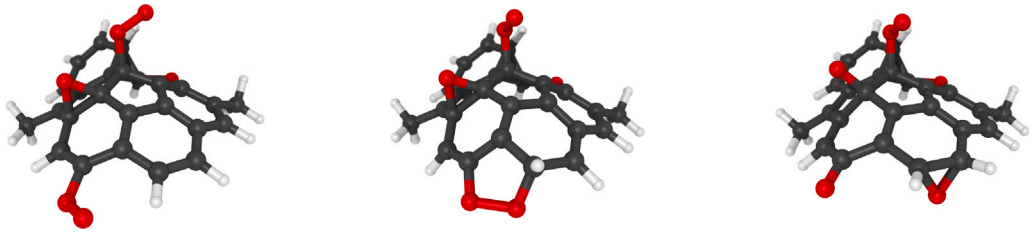


Fig. 8. Reaction profile of **B** with O(^{3}P) (Fig. 7). Reaction energies and barriers (TS) are given relative to the reactants at DFT TPSSh-D3/def-TZVP level in kJ/mol. The light gray lines mark the direct addition of atomic oxygen at different sites.

reaction profile in Fig. 12, shows that for **D** the initial barrier for the peroxo bridge is almost 58.0 kJ/mol lower and the barrier for breaking the O-O bond is 30.2 kJ/mol higher. Still, the overall formation energy of the epoxide of −166.8 kJ/mol is close to the value found for **C**. These results indicate that the formation of epoxides via arylperoxo intermediates is a general mechanism for the formation of epoxides in char, although the barrier heights and reaction energies depend on the electronic and molecular structure and, in particular, on the flexibility of the latter in the region of the reaction site.

3.2. Lactone formation

A pathway for the decomposition of epoxides in the vicinity of ether groups, *e.g.*, pyran rings, is the rearrangement to a lactone followed by



(a) 0.04 ps: **C1**: Oxygen addition.

(b) 0.54 ps: **C2**: Oxygen bridging.

(c) 3.05 ps: **C3**: Epoxide formation.

Fig. 9. Epoxide formation mechanism observed in the GFN2-xTB nanoreactor simulation of system **C** in O_2 atmosphere at 1500 K. The O_2 molecules are not illustrated for clarity.

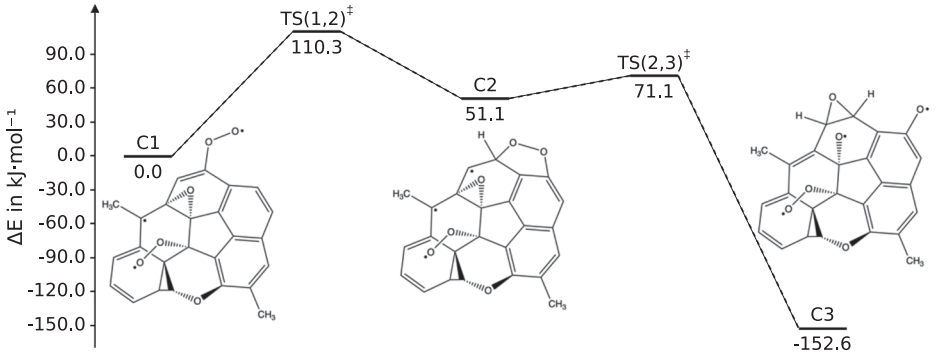
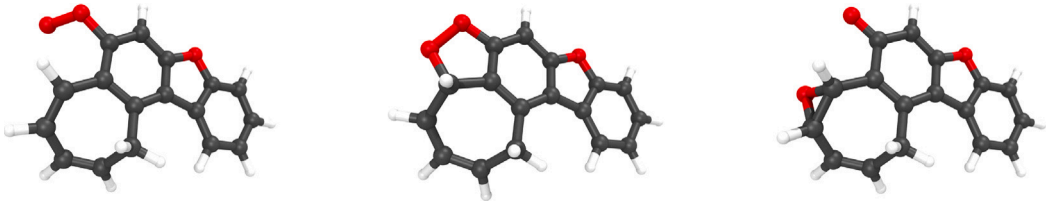


Fig. 10. Reaction profile of the epoxide formation in system **C**. All intermedieates are in a quartet state ($M_S = 4$). Reaction and activation barriers are given relative to **C** in kJ/mol at DFT TPSSh-D3/def-TZVP level.



(a) **D1**: Oxygen addition.

(b) **D2**: Oxygen bridging.

(c) **D3**: Epoxide formation.

Fig. 11. Molecular geometries of subspecies **D1**-**D3**, derived from test system **D**, optimized at DFT TPSSh-D3/def-TZVP level.

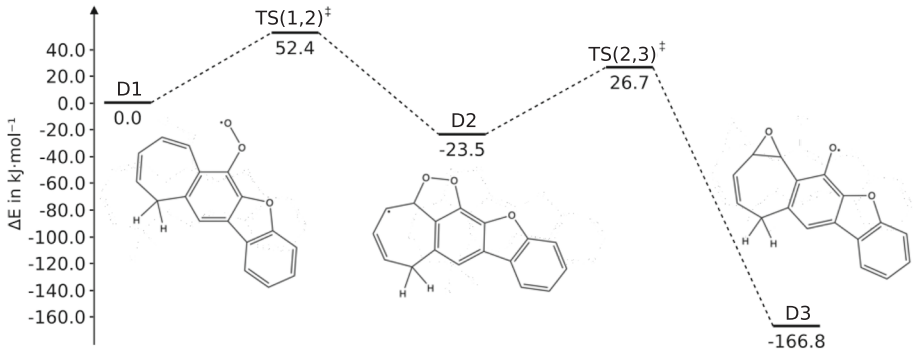
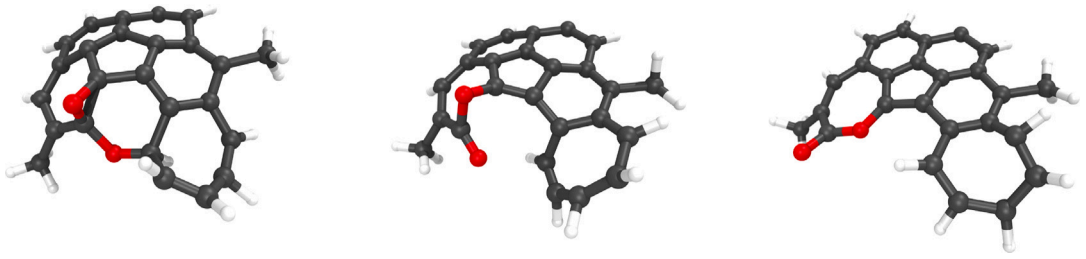


Fig. 12. Reaction profile of the epoxy group formation in system **D**. All systems are in a doublet state ($M_S = 2$). Reaction and activation barriers are given relative to **D1** in kJ/mol at DFT TPSSh-D3/def-TZVP level.



(a) 87.08 ps: Epoxide migration. (b) 87.29 ps: Lactone formation. (c) 87.40 ps: Lactone relaxation.

Fig. 13. Lactonization event observed for system **C** in vacuum at 2000 K.

a subsequent ring opening reaction. This mechanism was for example observed for model system **B** (Fig. 7), where this pathway leads to the formation of a highly reactive terminal carbon radical center. A similar reaction pathway was found in the MD simulations of model system **C** in vacuum at 2000 K. The corresponding snapshots are shown in Fig. 13. No lactone formation was observed in MD simulations at 1500 K. This is in good agreement with the hypothesis proposed by Levi et al. [5], that at elevated temperatures, epoxides rearrange to form ether and lactone groups as inferred from the increased lactone signal in XPS spectra of raw char. Decomposition pathways of lactones were previously studied with electronic structure calculations by Yönder et al. [70] who investigated the effect of the lactone group during high-temperature combustion. They reported that lactones eliminate CO_2 or undergo ring-opening reactions. Similar findings were also reported in a ReaxFF and DFT study by Xiang et al. [71].

3.3. XPS shifts of epoxides and ether

Levi et al. [5] and Barinov et al. [72] reported DFT results for oxygen 1*s* core-level shifts using Koopman's theorem which they used to identify epoxy groups in oxidized carbonaceous compounds by comparing the calculated shifts with experimental XPS spectra. To compare with their results, we computed O 1*s* core-level shifts of ether and epoxy groups using Koopmans' theorem. For this analysis, we included all ether groups from system **B** along with a number of aliphatic and mixed aliphatic-aromatic ether species for comparison. For a summary of the individual systems and computed shifts the reader is directed to Fig. 14. Shifts are reported relative to the core binding energy for the epoxy oxygen in the **M24 epoxy** model used as a reference in Ref. [5]. In the present work we re-optimized for consistency the structure of the **M24 epoxy** model with DFT/TPSSh-D3/def-TZVP.

For the epoxy groups located near the edge of system **B** the O 1*s* core binding energies are below the value for the **M24 epoxy** reference, with an average shift of −0.20 eV at the TPSSh-D3/cc-pV5Z level. Levi et al. [5] report for the O 1*s* core-level shifts of ethers a range of 0.2–1.5 eV relative to the **M24 epoxy** reference.

As seen in Fig. 14, the results from the present work support the conclusion that aromatic ether groups exhibit positive shifts relative to epoxides. In addition to the aromatic ethers, we determined O 1*s* core level shifts also for dimethyl ether (DME) and the **M24 ether** model from Ref. [5], which represent non-aromatic ether groups. In the **M24 ether** model the O atom is part of a seven-membered ring with a non-aromatic π-system, while DME is a purely aliphatic ether. While the O 1*s* core level shift for the **M24 ether** model is at the lower end of the range for ethers reported by Levi et al. [5] and still above the values for epoxides, the O 1*s* binding energy for the aliphatic DME is below that of the **M24 epoxy** reference and overlaps with the range obtained in the present work for epoxides. These results show that determining the exact nature of oxygen functional groups in coal and chars by XPS spectroscopy remains a challenging task, particularly when both aromatic and aliphatic ether groups are present.

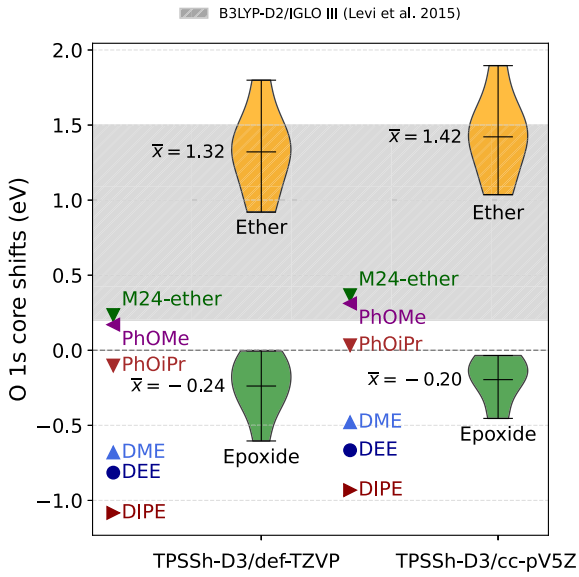


Fig. 14. Core-level O 1*s* binding energy shifts (in eV) for different epoxide and ether groups given relative to the reference epoxide system from Ref. [5]. The shifts were computed using Koopmans' theorem at the DFT TPSSh-D3 level with the def-TZVP and cc-pV5Z basis set. Shifts for the epoxide and ether groups studied in the present work are presented in violin plots next to their mean $\bar{x}$. For comparison, shifts of additional ethers are displayed as separate data points (diisopropyl ether (DIPE), diethyl ether (DEE), dimethyl ether (DME), 1-methylethoxybenzene (PhOiPr), anisol (PhOMe), and the M24-ether from Ref. [5].

4. Conclusion

Using an automated, MD simulation-driven reaction discovery workflow, we identified two epoxide formation mechanisms in char-derived systems. The first mechanism is initiated by O_2–addition to aryl radical sites and the second one by direct addition of $O(^3P)$ to unsaturated carbon groups. While previous studies suggested the possibility of these initial reaction steps, our approach eliminates most sources of human guesswork in the derivation of these. We were able to thermodynamically characterize the evolution of the nascent epoxides up to their eventual decomposition. A particular evolution path we observed, was the migration of epoxides to the edge of five-membered carbon rings, forming pyrans and reducing ring strain in the process. A second epoxide can migrate by similar mechanisms into the vicinity of such a pyran ring and transform it into a lactone group. The latter two evolution mechanisms are overall exothermic. Furthermore, the low energy barriers obtained for the migration steps substantiate the previously postulated role of epoxides as oxygen reservoirs in char. These results provide insight into the possible fate of epoxide species in the combustion of char.

The comparison of computed 1*s* core-level shifts for the investigated epoxides with those of ethers supports the notion that the peaks of aromatic ethers will appear in XPS spectra at higher energies than those for epoxides. On the other hand, peaks belonging to aliphatic ethers and epoxides apparently overlap, which complicates an unequivocal identification of epoxides by XPS spectroscopy. The developed computational models can be employed as such or in modified form for future studies on epoxides. The presented workflow can be extended further to characterize other intermediate species formed during char pyrolysis or burnout. The core-level shifts obtained in the current work, can serve as a reference for experimental studies to facilitate the analysis of XPS spectra of ethers in char, especially to differentiate peaks belonging to aromatic ethers from those originating from aliphatic ethers and epoxides.

CRediT authorship contribution statement

Bastian Schnieder: Writing – original draft, Validation, Methodology, Investigation, Data curation, Conceptualization. **Babak Farhadi Jahromi:** Writing – original draft, Validation, Methodology, Investigation, Data curation, Conceptualization. **Rochus Schmid:** Writing – review & editing, Supervision, Project administration, Methodology, Funding acquisition. **Christof Hättig:** Writing – original draft, Validation, Supervision, Project administration, Methodology, Funding acquisition, Data curation, Conceptualization.

Declaration of competing interest

The authors declare the following financial interests/personal relationships which may be considered as potential competing interests:

Bastian Schnieder reports that financial support was provided by the German Research Foundation. If there are other authors, they declare that they have no known competing financial interests or personal relationships that could have appeared to influence the work reported in this paper.

Acknowledgements

The authors thank the German Research Foundation (DFG) for funding this study within the framework of the SFB/Transregio 129 Oxyflame (Project number 215035359).

Data availability

The DFT-optimized geometries along with the electronic energies of the reactants, products and transition states of the studied reactions are available in a Zenodo repository [25] or on request from the authors.

References

[1] Lisý M, Lisá H, Jecha D, Baláš M, Križan P. Characteristic properties of alternative biomass fuels. Energies 2020;13(6). https://doi.org/10.3390/en13061448
[2] Pachauri N, Ahn CW, Choi TJ. Biochar energy prediction from different biomass feedstocks for clean energy generation. Environmental Technology & Innovation 2025;37:104012. https://doi.org/10.1016/j.eti.2024.104012
[3] Monfort MD, Sandhaas A, Zozmann E, Pönisch C, Kray D, Hartmann N. Energy system transformations toward zero emissions: a focus on pyrolysis. Energy Convers Manag 2025;X:101052.
[4] Shanmugam V, Sreenivasan S, Mensah RA, Försth M, Sas G, Hedenqvist MS, Neisiany RE, Tu Y, Das O. A review on combustion and mechanical behaviour of pyrolysis biochar. Mater Today Commun 2022;31:103629. https://doi.org/10.1016/j.mtcomm.2022.103629
[5] Levi G, Senneca O, Causá M, Salatino P, Lacovig P, Lizzit S. Probing the chemical nature of surface oxides during coal char oxidation by high-resolution XPS. Carbon 2015;90:181–96. https://doi.org/10.1016/j.carbon.2015.04.003
[6] Cerciello F, Forgione A, Lacovig P, Lizzit S, Fabozzi A, Salatino P, Senneca O. The influence of mineral matter on X-Ray photoelectron spectroscopy characterization of surface oxides on carbon. Appl Sci 2025;15(6). https://doi.org/10.3390/app15062993
[7] Janu R, Mrlik V, Ribitsch D, Hofman J, Sedláček P, Bielská L, Soja G. Biochar surface functional groups as affected by biomass feedstock, biochar composition and pyrolysis temperature. Carbon Resources Conversion 2021;4:36–46. https://doi.org/10.1016/j.crcon.2021.01.003
[8] Miller BG. 4 - introduction to coal utilization technologies. In Miller BG, editor. Clean coal engineering technology (second edition). 2nd Edition, Butterworth-Heinemann; 2017. pp. 147–229. https://doi.org/10.1016/B978-0-12-811365-3.00004-1
[9] Saastamoinen J, Tourunen A. Model for char combustion, particle size distribution, and inventory in AIR and oxy-fuel combustion in fluidized beds. Energy Fuels 2012;26(1):407–16. https://doi.org/10.1021/ef201362h
[10] Khalil AE, Gupta AK. Hydroxyl radical distribution in distributed reaction combustion condition. Fuel 2014;122:28–35. https://doi.org/10.1016/j.fuel.2014.01.010
[11] Kohse-Höinghaus K. Combustion, chemistry, and carbon neutrality. Chem Rev 2023;123(8):5139–219. https://doi.org/10.1021/acs.chemrev.2c00828
[12] Cerciello F, Coppola A, Lacovig P, Senneca O, Salatino P. Characterization of surface-oxides on char under periodically changing oxidation/desorption conditions. Renewable Sustain Energy Rev 2021;137:110453. https://doi.org/10.1016/j.rser.2020.110453.
[13] Incze A, Pasturel A, Chatillon C. First-principles study of the atomic oxygen adsorption on the (0 0 0 1) graphite surface and dissolution. Appl Surf Sci 2001;177(4):226–9. https://doi.org/10.1016/s0169-4332(01)00216-1
[14] Sánchez A, Mondragón F. Role of the epoxy group in the heterogeneous CO_2 evolution in carbon oxidation reactions. J Phys Chem C 2006;111(2):612–7. https://doi.org/10.1021/jp065701i
[15] Orrego JF, Zapata F, Truong TN, Mondragón F. Heterogeneous CO_2 evolution from oxidation of aromatic Carbon-Based materials. J Phys Chem A 2009;113(29):8415–20. https://doi.org/10.1021/jp903362g
[16] Radovic LR, Silva-Tapia AB, Vallejos-Burgos F. Oxygen migration on the graphene surface. 1. Origin of epoxide groups. Carbon 2011;49(13):4218–25. https://doi.org/10.1016/j.carbon.2011.05.059
[17] Radovic LR, Suarez A, Vallejos-Burgos F, Sofo JO. Oxygen migration on the graphene surface. 2. Thermochemistry of basal-plane diffusion (hopping). Carbon 2011;49(13):4226–38. https://doi.org/10.1016/j.carbon.2011.05.037
[18] Schmitz G, Yönder O, Schnieder B, Schmid R, Hättig C. An automatized workflow from molecular dynamic simulation to quantum chemical methods to identify elementary reactions and compute reaction constants. J Comput Chem 2021;42(32):2264–82. https://doi.org/10.1002/jcc.26757
[19] Wood R, Mašek O, Erastova V. Developing a molecular-level understanding of biochar materials using public characterization data. Cell Rep Phys Sci 2024;5(7):102036. https://doi.org/10.1016/j.xcrp.2024.102036
[20] Senftle TP, Hong S, Islam MM, Kylasa SB, Zheng Y, Shin YK, Junkermeier C, Engel-Herbert R, Janik MJ, Aktulga HM, Verstraelen T, Grama A, van Duin ACT. The ReaxFF reactive force-field: development, applications and future directions. npj Comput Mater 2016;2(1) (Mar). https://doi.org/10.1038/npjcompumats.2015.11
[21] Bannwarth C, Ehlert S, Grimme S. GFN2-xTB—an accurate and broadly parametrized Self-Consistent Tight-Binding quantum chemical method with multipole electrostatics and Density-Dependent dispersion contributions. J Chem Theory Comput 2019;15(3):1652–71. https://doi.org/10.1021/acs.jctc.8b01176
[22] Hong D, Liu L, Wang C, Si T, Guo X. Construction of a coal char model and its combustion and gasification characteristics: molecular dynamic simulations based on reaxff. Fuel 2021;300:120972. https://doi.org/10.1016/j.fuel.2021.120972
[23] Li X, Zheng M, Ren C, Guo L. Reaxff molecular dynamics simulations of thermal reactivity of various fuels in pyrolysis and combustion. Energy & Fuels 2021;35(15):11707–39. https://doi.org/10.1021/acs.energyfuels.1c01266
[24] Bhoi S, Banerjee T, Mohanty K. Molecular dynamic simulation of spontaneous combustion and pyrolysis of brown coal using reaxff. Fuel 2014;136:326–33. https://doi.org/10.1016/j.fuel.2014.07.058
[25] Schnieder B, Jahromi BF, Schmid R, Hättig C. Raw data to computational study toward the formation, migration, and conversion of epoxy groups during combustion of char. 2025. https://doi.org/10.5281/zenodo.15835120
[26] Cong Y, Zhai Y, Chen X, Li H. The accuracy of Semi-Empirical quantum Chemistry methods on soot formation simulation. Int J Mol Sci 2022;23(21). https://doi.org/10.3390/ijms232113371
[27] Perry DL, Grint A. Application of XPS to coal characterization. Fuel, 1983;62(9):1024–33. society of Chemical Industry Conference, Analytical Methods for Coals, Cokes and Carbons. https://doi.org/10.1016/0016-2361(83)90135-7
[28] Desimoni E, Casella GI, Morone A, Salvi AM. XPS determination of oxygen-containing functional groups on carbon-fibre surfaces and the cleaning of these surfaces. Surf Interface Anal 1990;15(10):627–34. https://doi.org/10.1002/sia.740151011
[29] Angenent V, Oelert D, Schmid R. Towards realistic structural char models: generation of stacked graphene-like layers using constrained reactive molecular dynamics simulations. Fuel 2024;372:132064. https://doi.org/10.1016/j.fuel.2024.132064
[30] Angenent V. Silico design of atomistic char models for gas adsorption and combustion, [Ph.D. thesis], Ruhr-Universität Bochum; 2023.
[31] Hu W-P, Rossi I, Corchado JC, Truhlar DG. Molecular modeling of combustion kinetics. The abstraction of primary and secondary hydrogens by hydroxyl radical. J Phys Chem A 1997;101(37):6911–21. https://doi.org/10.1021/jp970188h
[32] Xi Z, Suo L, Xia T. Characterization of elementary reactions inducing coal spontaneous combustion. Fuel 2024;358:130138. https://doi.org/10.1016/j.fuel.2023.130138
[33] Thompson AP, Aktulga HM, Berger R, Bolintineanu DS, Brown WM, Crozier PS, in 't Veld PJ, Kohlmeyer A, Moore SG, Nguyen TD, Shan R, Stevens MJ, Tranchida J, Trott C, Plimpton SJ. LAMMPS - a flexible simulation tool for particle-based materials modeling at the atomic, meso, and continuum scales. Comp Phys Comm 2022;271:108171. https://doi.org/10.1016/j.cpc.2021.108171
[34] Schmid R. Pylmps; 2024. https://github.com/MOFplus/cmc-tools.git [accessed: May 2025].

[35] Bannwarth C, Caldeweyher E, Ehlert S, Hansen A, Pracht P, Seibert J, Spicher S, Grimme S. Extended tight-binding quantum Chemistry methods, wiley interdiscip. Rev Comput Mol Sci 2021;11(2) (Mar). https://doi.org/10.1002/wcms.1493
[36] Martínez L, Andrade R, Birgin EG, Martínez JM. PACKMOL a package for building initial configurations for molecular dynamics simulations. J Comput Chem 2009;30(13):2157–64. https://doi.org/10.1002/jcc.21224
[37] Grimme S. Exploration of chemical compound, conformer, and reaction space with Meta-Dynamics simulations based on Tight-Binding quantum chemical calculations. J Chem Theory Comput 2019;15(5):2847–62. https://doi.org/10.1021/acs.jctc.9b00143
[38] Berendsen HJC, Postma JPM, van Gunsteren WF, DiNola A, Haak JR. Molecular dynamics with coupling to an external bath. J Chem Phys 1984;81(8):3684–90. https://doi.org/10.1063/1.448118
[39] Nosé S. A molecular dynamics method for simulations in the canonical ensemble. Mol Phys 1984;52(2):255–68. https://doi.org/10.1080/00268978400101201
[40] Nosé S. A unified formulation of the constant temperature molecular dynamics methods. J Chem Phys 1984;81(1):511–9. https://doi.org/10.1063/1.447334
[41] Hoover WG. Canonical dynamics: equilibrium phase-space distributions. Phys Rev A 1985;31(3):1695–7. https://doi.org/10.1103/physreva.31.1695
[42] Martyna GJ, Klein ML, Tuckerman M. Nosé–hoover chains: the canonical ensemble via continuous dynamics. J Chem Phys 1992;97(4):2635–43. https://doi.org/10.1063/1.463940
[43] Grimme S, Antony J, Ehrlich S, Krieg H. A consistent and accurate AB initio parametrization of density functional dispersion correction (DFT-d) for the 94 elements H-Pu. J Chem Phys 2010;132(15):154104. https://doi.org/10.1063/1.3382344
[44] TURBOMOLE V7.6. A development of university of karlsruhe and forschungszentrum karlsruhe GmbH, 1989–2007. TURBOMOLE GmbH, since 2007; available from, 2022. http://www.turbomole.com [accessed: 7 January 2025].
[45] Zhao Y, Truhlar DG. Density functional theory for reaction energies: test of meta and hybrid meta functionals, Range-Separated functionals, and other High-Performance functionals. J Chem Theory Comput 2011;7(3):669–76. https://doi.org/10.1021/ct1006604
[46] Eichkorn K, Treutler O, Öhm H, Häser M, Ahlrichs R. Auxiliary basis sets to approximate Coulomb potentials (chem. Phys. Letters 240 (1995) 283-290). Chem Phys Lett 1995;242(6):652–60. https://doi.org/10.1016/0009-2614(95)00838-U
[47] Eichkorn K, Weigend F, Treutler O, Ahlrichs R. Auxiliary basis sets for main row atoms and transition metals and their use to approximate Coulomb potentials. Theor Chem Acc 1997;97(1):119–24. https://doi.org/10.1007/s002140050244
[48] Grimme S, Antony J, Ehrlich S, Krieg H. A consistent and accurate AB initio parametrization of density functional dispersion correction (DFT-d) for the 94 elements H-Pu. J Chem Phys 2010;132(15):154104. https://doi.org/10.1063/1.3382344
[49] Tao J, Perdew JP, Staroverov VN, Scuseria GE. Climbing the density functional ladder: nonempirical meta–generalized gradient approximation designed for molecules and solids. Phys Rev Lett 2003;91:146401. https://doi.org/10.1103/PhysRevLett.91.146401
[50] Schäfer A, Horn H, Ahlrichs R. Fully optimized contracted Gaussian basis sets for atoms Li to Kr. J Chem Phys 1992;97(4):2571–7. https://doi.org/10.1063/1.463096
[51] Staroverov VN, Scuseria GE, Tao J, Perdew JP. Comparative assessment of a new nonempirical density functional: molecules and hydrogen-bonded complexes. J Chem Phys 2003;119(23):12129–37. https://doi.org/10.1063/1.1626543
[52] Schäfer A, Huber C, Ahlrichs R. Fully optimized contracted Gaussian basis sets of triple zeta valence quality for atoms li to kr. J Chem Phys 1994;100(8):5829–35. https://doi.org/10.1063/1.467146
[53] Csonka GI, Ruzsinszky A, Perdew JP. Estimation, computation, and experimental correction of molecular zero-point vibrational energies. J Phys Chem A 2005;109(30):6779–89. https://doi.org/10.1021/jp0519464
[54] Plessow P. Reaction path optimization without NEB springs or interpolation algorithms. J Chem Theory Comput 2013;9(3):1305–10.
[55] Helgaker T. Transition-state optimizations by trust-region image minimization. Chem Phys Lett 1991;182(5):503–10. https://doi.org/10.1016/0009-2614(91)90115-P
[56] Hellweg A. Heuristic control of kinetic energy in dynamic reaction coordinate calculations. J Comput Chem 2013;34(21):1835–41. https://doi.org/10.1002/jcc.23332
[57] Tsuneda T, Song J-W, Suzuki S, Hirao K. On koopmans' theorem in density functional theory. J Chem Phys 2010;133(17):174101. https://doi.org/10.1063/1.3491272
[58] Bellafont NP, Illas F, Bagus PS. Validation of koopmans' theorem for density functional theory binding energies. Phys Chem Chem Phys 2015;17:4015–9. https://doi.org/10.1039/C4CP05434B
[59] Peterson KA, Woon DE, Dunning J, Thom H. Benchmark calculations with correlated molecular wave functions. IV. The classical barrier height of the H + H2→H2 + H reaction. J Chem Phys 1994;100(10):7410–5. https://doi.org/10.1063/1.466884
[60] Humphrey W, Dalke A, Schulten K. VMD: visual molecular dynamics. J Mol Graph 1996;14(1):33–8. https://doi.org/10.1016/0263-7855(96)00018-5
[61] Stone J. An efficient library for parallel ray tracing and animation, [Master's thesis], Computer Science Department, University of Missouri-Rolla. Apr 1998.
[62] I. Revvity Signals Software. ChemDraw professional, Software, version 22.2 (2024. https://revvitysignals.com/products/research/chemdraw.
[63] Angnes RA. Ricalmang/mechaSVG v.0.0.8; 2020. https://doi.org/10.5281/ZENODO.4065333. https://zenodo.org/record/4065333.
[64] Zheng Q, Zhang D, Fu P, Wang A, Sun Y, Li Z, Fan Q. Insight into the fast pyrolysis of lignin: unraveling the role of volatile evolving and char structural evolution. Chem Eng J 2022;437:135316. https://doi.org/10.1016/j.cej.2022.135316
[65] Gaydon A. The role of atomic oxygen in combustion. Trans Faraday Soc 1946;42:292–5.
[66] Du Z, Sarofim AF, Longwell JP, Mims CA. Kinetic measurement and modeling of carbon oxidation. Energy & Fuels 1991;5(1):214–21. https://doi.org/10.1021/ef00025a035
[67] Levi G, Causá M, Lacovig P, Salatino P, Senneca O. Mechanism and thermochemistry of coal char oxidation and desorption of surface oxides. Energy & Fuels 2017;31(3):2308–16. https://doi.org/10.1021/acs.energyfuels.6b02324
[68] Wal RLV, Bryg VM, Hays MD. XPS analysis of combustion aerosols for chemical composition, surface chemistry, and carbon chemical state. Anal Chem 2011;83(6):1924–30. https://doi.org/10.1021/ac102365s
[69] Yuan W, Li Y, Qi F. Challenges and perspectives of combustion Chemistry research. Science China Chemistry 2017;60(11):1391–401. https://doi.org/10.1007/s11426-017-9066-9
[70] Yönder Ö, Schmitz G, Schmid R, Schnieder B, Hättig C. A computational Chemistry study on the evolution of oxygen functional groups during char burnout. Fuel 2024;365:131217. https://doi.org/10.1016/j.fuel.2024.131217
[71] Xiang Z, Acikel MB, Hansen CJ, Jeong G-U, Pérez-Soto R, Wang DZ, Whoriskey VC, Kim S, McEnally CS, Pfefferle LD, Xuan Y. The sooting behavior of lactones as sustainable fuels. Sustain Energy Fuels 2024;8:5206–13. https://doi.org/10.1039/D4SE00883A
[72] Barinov A, Malciočlu OB, Fabris S, Sun T, Gregoratti L, Dalmiglio M, Kiskinova M. Initial stages of oxidation on graphitic surfaces: photoemission study and density functional theory calculations. J Phys Chem C 2009;113(21):9009–13. https://doi.org/10.1021/jp902051d